Modeling counter-current spontaneous imbibition and its scaling application to underground gas storage

by

Shaluka Rajantha Senevirathna

B.S., University of Peradeniya, 2020

A THESIS

submitted in partial fulfillment of the requirements for the degree

MASTER OF SCIENCE

Department of Geology
College of Arts and Sciences

KANSAS STATE UNIVERSITY
Manhattan, Kansas

2024

Approved by:

Major professor
Dr. Behzad Ghanbarian

Copyright

Abstract

Spontaneous imbibition (SI) is a process by which a liquid (e.g., water or oil) is naturally drawn into a partially saturated porous medium under capillarity. Understanding the SI and its mechanisms have broad applications, particularly to underground gas storage in deep aquifers or depleted reservoirs. For instance, injecting CO_2 under the supercritical conditions into subsurface, known as CO_2 sequestration, is a practical solution to reduce greenhouse gases in the atmosphere and help fight climate change. Modeling and scaling the counter-current SI has been a long-standing issue, and various approaches have been proposed in the literature. In this study, to model the SI we generalize fractional flow theory (GFFT) using fractional derivatives and apply non-Boltzmann scaling. In our approach, the imbibition distance is proportional to the time to the power $\alpha/2$ in which α is fractional order ($0 < \alpha < 2$). We analyzed the SI data reported in literature including 25 sandstones, 2 diatomites, carbonates, clay samples, 6 synthetic porous media and silty clay soil samples. By plotting the normalized liquid recovery against the dimensionless time, we found that the non-Boltzmann transformation (variable α) yielded a better collapse in the SI data than the Boltzmann transformation (α = 1). More specifically, results showed that α ranged between 0.88 and 1.54. Also, we fit the solution of GFFT to experimental and stimulation data reported in literature including soil, clay and carbonate samples to show that non-Boltzmann transformation model the SI resulting in variable α values accurately than the traditional Boltzmann approach (fixed α=1). We demonstrate that the variation in α value can be attributed to contact angle of the fluid, dynamic viscosity, fracture dynamics and pore structure. However, further investigations are still required. Using the GFFT, we expect to more accurately predict the rate and amount of fluid that can spontaneously imbibe into a porous medium if

characteristics such as porosity, permeability, initial and maximum saturations, viscosity, and wettability are known.

Keywords: Counter-current spontaneous imbibition, CO_2 sequestration, Fractional derivatives, Fractional flow, non-Boltzmann scaling

Table of Contents

List of Figures

List of Tables

Acknowledgements

I wish to extend my heartfelt appreciation to the Department of Geology at Kansas State University, particularly to Dr. Pamela Kempton, the Department Head, for their consistent support and provision of resources during my academic journey at K-State.

My deepest gratitude goes to my academic mentor, Dr. Behzad Ghanbarian, whose unwavering support has been invaluable from the inception to the conclusion of this research. Dr. Ghanbarian's dedication and profound insights have played a pivotal role in my academic endeavors.

I am also indebted to my advisory committee members, namely Dr. Anna Zemlynova, Dr. Abdelmoneam Raef, and Dr. Qinhong Hu, for their indispensable guidance, encouragement, and scholarly perspectives that have greatly enriched this research.

Special recognition is due to Emeritus Professor David B. McWhorter for his enlightening discussions on fractional flow theory, which laid the groundwork for this project's inception. Additionally, I extend my gratitude to my friends and colleagues for their various forms of support, encouragement, and camaraderie throughout this endeavor.

I am grateful to the funding sources, including the Graduate School and College of Arts and Sciences at Kansas State University, for their financial support and recognition of the significance of scientific inquiry, which made this research possible.

Finally, I express my appreciation to Kansas State University for providing an enriching academic environment conducive to my scholarly and research pursuits.

Dedication

I dedicate this thesis to my beloved father and mother back in my homeland of Sri Lanka, whose unwavering love, encouragement, and sacrifices have been the cornerstone of my academic journey. Their steadfast support has served as the guiding light throughout this endeavor. I recognize that this accomplishment is as much theirs as it is mine.

Additionally, I extend my gratitude to all the teachers who have guided me throughout my education, from my earliest years of childhood to the completion of my bachelor's degree back in Sri Lanka. Their dedication to imparting knowledge has been instrumental in shaping my academic path.

I am also thankful to all the individuals who contributed through their taxes to support the educational system in Sri Lanka, which enabled me to pursue my bachelor's degree. It is their collective investment in education that laid the foundation for my journey to attain a master's degree at the United States.

Chapter 1 - Introduction

Spontaneous imbibition (SI) is a crucial process through which a wetting phase (e.g., water) enters spontaneously into a porous medium replace or displace a non-wetting phase (e.g., air) under capillary forces (Schmid and Geiger, 2012). The SI is primarily influenced by rock wettability, permeability, initial water content, viscosity, and pore structure (Zahasky and Benson, 2019). There exist two types of the SI: (1) counter-current and (2) co-current (Standnes, 2004). In the counter-current SI, non-wetting and wetting fluids flow in opposing directions, while in the co-current one, both fluids move along the same direction. Counter-current SI is considered the predominant driving mechanism among the two modes, as evidenced by the extensive experimental and computational studies on this topic.

1.1 SI and its modeling

The literature on the SI is vast and extensive (Mason and Morrow, 2013). Experimental approaches (Gao and Hu, 2016; Pan et al., 2022), theoretical models (Cai et al., 2014; Liu et al., 2016), numerical simulations (Behbahani et al., 2006; Liu et al., 2020) and artificial intelligence-based models (Deng and Pan, 2021; Mahdaviara et al., 2022) were widely applied to study the SI in porous media, particularly tight rocks (Sun et al., 2017), coals (Liu et al., 2021) and fracture networks (Gong and Rossen, 2018). For a review, see Abd et al. (2019).

Among theoretical approaches, several models were developed based on bundle of capillary tubes approach, an oversimplifying idealization of a porous medium in which the network of pores is replaced with non-interconnected tortuous tubes spanning the entire medium. For instance, Cai et al. (2014) proposed a model for the SI based on the bundle of capillary method. In another study, Shi et al. (2018) developed a theoretical model without considering hydrostatic pressure and a semi-analytical model with considering hydrostatic pressure using the bundle of capillary tubes in combination with fractal theory. However, those authors did not evaluate their derivations via either experiments or simulations.

1.2 Scaling analysis of SI

Understanding SI characteristics across rocks with varying properties and generalizing insights about the imbibition phenomenon is essential for the scaling analysis of SI. Scaling laws or models are derived to represent oil recovery from a specific rock sample in relation to dimensionless time (Standnes, 2004). Scaling the counter-current SI data for various porous media has been a long-standing issue, and multiple approaches have been proposed in the literature.

As the first attempt to scale SI data, Mattax and Kyte (1962) introduced a mathematical framework for SI that integrated both gravitational and capillary forces based on upon the framework of Rapoport (1955), introducing a dimensionless time (Abd et al., 2019). This model considered capillarity, gravitational effects on fluid saturation, viscosity, and core dimensions (Cai et al., 2021). Subsequent to Mattax and Kyte (1962)'s work, several other scaling laws emerged, with Ma et al. (1997) contributing a significant advancement. Their relation introduced a new characteristic length into the scaling law, accommodating various boundary conditions and leading to the development of a new scaling relationship (Abd et al., 2019).

The model developed by Ma et al. (1997) was applicable only for specific conditions such as with same wettability, identical relative permeabilities, gravity less condition etc. and works well with oil/water/rock systems (Kewen and Roland, 2006). Zhang et al. (1996) showed that the model by Ma et al. (1997) fails to scale SI data of gas/liquid/rock systems and to overcome this Li and Horne (2004) developed a model which could scale counter-current SI data into gas saturated porous media (Kewen and Roland, 2006).

While the literature boasts a range of SI models, many have inherent limitations. Many need to pay more attention to critical factors like capillary pressure, relative permeability, and wettability, thereby constraining their broader applicability. Recognizing these limitations, several researchers have endeavored to integrate capillarity and permeability effects or introduce supplementary assumptions to craft more encompassing models (Schmid and Geiger, 2012). Consequently, while numerous models exist, their universal applicability across diverse porous media types still needs to be improved.

A theoretic framework proposed to scale the counter-current SI is based on fractional flow theory. Schmid and Geiger (2012) applied fractional flow theory, first developed by Buckley and Leverett (1942), in combination with the Boltzmann transformation ($x = \lambda t^{0.5}$ in which x is the distance, t is the time, and λ is a numerical prefactor) to model the SI. To evaluate their approach, Schmid and Geiger (2012) used 42 datasets including water-oil and water-air experiments in which water was the wetting phase.

Although the Boltzmann scaling has been widely applied in the literature to characterize the SI, several studies showed deviations from the exponent 0.5 in the Boltzmann transformation. For instance, Hu et al. (2012) reported three types of imbibition slopes, which differ from 0.5 (Gao and Hu, 2023). They performed experimental approaches as well as network modeling to show that porous media with low pore connectivity exhibits low imbibition slopes such as 0.26 (Hu et al., 2012). Kelly (2015) reported experimental results based on nanofluidic chips with parallel nanochannels and used image and data analysis schemes to show the deviation of imbibition time exponents from 0.5, specifically for nano-porous media. They showed that imbibition in nanochannels is at least five times slower than predicted by the Washburn equation (Kelly, 2015). Also, Ning et al. (2022), using the concepts of percolation theory, showed that the imbibition rate is influenced by the fracture parameters and connectivity between grid cells. These results suggest that the imbibition process is affected by various factors, including the fluid's viscosity and temperature, the material's wettability, fracture distribution, pore structure, boundary conditions like initial saturation, maximum saturation etc. (Gao and Hu, 2023).

Chapter 2 - Objectives

There exist evidence including experimental measurements and numerical simulations in the literature that strongly suggest deviations from the Boltzmann scaling at both pore (Kelly et al., 2015; Zhao et al., 2021; Cai et al., 2022) and core (Hu et al., 2001; Hu et al., 2012; Pan et al., 2021; Zhao et al., 2022) scales. In addition to that, although various approaches were proposed to scale counter-current SI data, normalized recovery factors and/or saturation degrees versus some dimensionless time still do not perfectly collapse onto a universal curve (Schmid and Geiger, 2012). The main objectives of this study, therefore, are to: (1) develop a new model for the counter-current SI by generalizing fractional flow theory using fractional derivatives and non-Boltzmann transformation, (2) present a novel scaling law to better collapse SI data, and (3) evaluate the proposed approaches using experimental and numerical data for different types of porous media.

In the following we focus on countercurrent SI, and for the sake of simplicity we denote it as SI.

Chapter 3 - Theory

3.1 Fractional flow theory

Buckley and Leverett (1942) presented the fractional flow theory to describe the physics of immiscible displacements in porous media. After their pioneering work, Mcwhorter and Sunada (1990) presented exact quasi-analytical solutions for both one-dimensional and radial flow of two incompressible fluids and calculated their fractional-flow functions for the first time.

The partial differential equation for the one-dimensional horizontal flow of two immiscible and incompressible fluids is (Mcwhorter and Sunada, 1990)

$$\phi \frac{\partial S_w}{\partial t} = -q_t \frac{\Delta f(S_w)}{\Delta S_w} \frac{\partial}{\partial x} S_w + \frac{\partial}{\partial x}\left(D(S_w) \frac{\Delta P_c}{\Delta S_w} \frac{\partial S_w}{\partial t}\right) \tag{1}$$

where S_w is the wetting-phase saturation, t is the time, q_t is the total volume flux, P_c is the capillary pressure, ϕ is the porosity, and D is the diffusivity coefficient, and f is the fractional flow function which describes the flow rate of a fluid to the total flow rate. D and f are expressed as follows (Mcwhorter and Sunada, 1990)

$$f(S_w) = \left[1 + \frac{k_{nw}\mu_w}{k_w\mu_{nw}}\right]^{-1} \tag{2a}$$

$$D(S_w) = -\frac{k_{nw} f(S_w)}{\mu_{nw}} \frac{\Delta P_c}{\Delta S_w} \tag{2b}$$

where k_w and k_{nw} are respectively the wetting- and non-wetting-phase permeabilities, and μ_w and μ_{nw} are the wetting and non-wetting-phase dynamic viscosities, respectively.

In the case of counter-current SI, the total flux (q_t) is zero because the volume flux of the wetting phase is equal to that of the non-wetting phase (q_w = -q_{nw}), and, thus, Eq. (1) reduces (Schmid, 2012),

$$\phi \frac{\partial S_w}{\partial t} = \frac{\partial}{\partial x}\left(D(S_w) \frac{\partial S_w}{\partial x}\right) \tag{3}$$

3.2 Generalized fractional flow theory

Fractional derivatives have been recently used widely to model transport phenomena in porous media (Meerschaert and Sikorskii, 2019) and to study two-phase flow in porous rocks (Li et al., 2022). Using concepts of time fractional calculus, we generalize fractional flow theory

$$\phi \frac{\partial S_w}{\partial t^\alpha} = \frac{\partial}{\partial x}\left[D_\alpha^F(S_w)\frac{\partial S_w}{\partial x}\right] \tag{4}$$

where α is the fractional order of the partial derivative (Pachepsky et al., 2003).

Theoretically, the exponent α ranges between 0 and 2 (Sun et al., 2013), and for $\alpha = 1$ the GFFT, Eq. (4), reduces to Eq. (3). We should point out that Eq. (4) is similar in form to the time-fractional Richards' equation, Eq. (5). Note that, the effect of porosity (ϕ) is reflected in Eq. (4) in the GFFT, and it is not reflected in Eq. (5). The time fractional Richards' equation was first proposed by Pachepsky et al. (2003) and followed by Sun et al. (2013).

$$\frac{\partial S_w}{\partial t^\alpha} = \frac{\partial}{\partial x}\left[D_\alpha^R(S_w)\frac{\partial S_w}{\partial x}\right] \tag{5}$$

$$D_\alpha^R(S_w) = k_w \frac{\Delta P_c}{\Delta S_w} \tag{6}$$

Although Eq. (3) is similar in form to Richards' equation (Richards, 1931), the $D(S_w)$ in Eqs. (1) and (3), defined in Eq. (2b), is different from soil-water diffusivity Eq. (6) in Richards' equation. In fact, the $D(S_w)$ given by Eq. (2b) is a non-monotonic function of S_w (see Fig. 4b in Mcwhorter and Sunada (1990), while the $D(S_w)$ in Richards' equation monotonically increasing with increasing S_w. Therefore, the definitions of $D_\alpha^F(S_w)$ in Eq. (4) is different from that $D_\alpha^R(S_w)$ in Eq. (6) as well.

In the following, we apply the generalized fractional flow theory, GFFT, in combination with the non-Boltzmann transformation, $x = \lambda t^{\frac{\alpha}{2}}$, to model the counter-current SI. Using the fact that $\lambda = x t^{-\alpha/2}$ and the chain rule gives the following relationships

$$\frac{\partial S_w}{\partial t^\alpha} = \frac{dS_w}{d\lambda}\frac{\partial \lambda}{\partial t^\alpha} = -\frac{dS_w}{d\lambda}\frac{\lambda}{2t^\alpha} \tag{7}$$

$$\frac{\partial S_w}{\partial x} = \frac{dS_w}{d\lambda}\frac{\partial \lambda}{\partial x} = \frac{dS_w}{d\lambda}\frac{1}{t^{\alpha/2}} \tag{8}$$

Substituting (4) into the equation (8) produces a non-linear ordinary differential equation of the second order for the function $S_w = S_w(\lambda)$

$$-\phi\frac{\lambda}{2}\frac{\partial S_w}{\partial \lambda} = \frac{\partial}{\partial \lambda}\left[D_\alpha^F(S_w)\frac{\partial S_w}{\partial \lambda}\right] \tag{9}$$

Introducing new unknown functions as $z(\lambda) = S_w(\lambda)$ and $w(\lambda) = S_w{}'(\lambda)$, Eq (9) can be reduced to a pair of ordinary differential equations of the first order as follows,

$$z' = w \tag{10}$$

$$w' = -\frac{D_\alpha^{F\prime}(z)w^2 + \phi w\lambda/2}{D_\alpha^F(z)} \tag{11}$$

In a medium with some initial water saturation, one may set $S_w(t = 0) = S_i$. Eq (10) and (11) is subjected to following boundary conditions

$$S_w(x, t = 0) = S_w(\infty, t) = S_i \qquad z(\infty) = S_i \tag{12a}$$

$$S_w(x = 0, t) = S_0 \qquad z(0) = S_0 \tag{12b}$$

We should note that the proposed solution, Eqs. (10)-(11), is different from those developed by Pachepsky et al. (2003), Sun et al. (2013) and Li et al. (2022).

3.3 Scaling counter-current SI

In this section, we generalize the Schmid and Geiger (2012) approach by applying concepts of the GFFT and non-Boltzmann transformation. The cumulative imbibition of a wetting phase (Q_w) to a system can be calculated by $Q_w = 2At^{1/2}$ (Schmid and Geiger, 2012). We generalize it by introducing α and by introducing an additional boundary condition using q_w, the wetting flux at x=0 at given time in the system,

$$Q_w(t) = \int_0^t q_w(0,t)dt = 2At^{\alpha/2} \tag{13}$$

Since we are incorporating non-Boltzmann transformation in our study, $t^{1/2}$ becomes $t^{\alpha/2}$ in Eq. (13). A is a parameter which depends on the fluid-rock system properties and calculates as a part of the analytical solution for two phase flow by Mcwhorter and Sunada (1990). A depends on the porosity of the medium, the diffusivity and the fractional flow function (see Eq. 24 in Mcwhorter and Sunada (1990). t is time and α is the constant in the imbibition time exponent.

A characteristic length L_c, incorporating boundaries of the imbibition of fluids in the considered matrix, can be defined as follows (Ma et al., 1997),

$$L_c = \sqrt{\frac{V_b}{\sum_{i=1}^{n} a_i / l_{a_i}}} \tag{14}$$

where V_b is the porous medium bulk volume, a_i is the area that opens to the imbibition in i^{th} direction, and l_{ai} is the distance the imbibition front travels towards the no-flow boundary. Using Eq. (13), we generalize the Schmid and Geiger (2012) definition of dimensionless time, t_d, as follows

$$t_d = \left(\frac{2A}{\phi L_c}\right)^{2/\alpha} t \tag{15}$$

In which α is the fractional order in the GFFT, Eq. (4). We should point out that the proposed scaling approach reduces to that of Schmid and Geiger (2012) when $\alpha = 1$.

Chapter 4 - Material and Methods

4.1 Modeling counter-current SI

This study develops a new model for the SI based on the GFFT and present a novel modeling approach using the non-Boltzmann transformation to scale SI data in different types of rocks. The proposed model is evaluated with different types of porous media to ensure the accuracy and the general applicability of the model. In this work, with the utilization of the GFFT, a more precise prediction of the imbibition of fluid into a porous medium is expected when key characteristics such as porosity, permeability, initial and maximum saturations, viscosity, and wettability are known. We show that the GFFT predicts and captures the heterogeneity of the porous media in terms of fluid flow accurately than classical Richards' approach.

In this section, we briefly describe various sets of experiments and simulations collected from the literature. Next, we explain how the GFFT was fit to the data using a Python code and how the exponent α was optimized.

4.1.1 Ferguson and Gardner (1963) dataset

We analyzed data from Ferguson and Gardner (1963) who measured time needed for waterfront to reach locations along a soil column. Their experiments were conducted on a Salkum silty clay sample prepared non-destructively. They measured and reported the water content as a function of time at various places along the soil column starting from 3.5cm up to 27.5cm using a gamma ray absorption equipment to measure the water content as a function of time. In this study, we fit our solution of GFFT to the water saturation curves (Originally reported in terms of water content Q) to show that GFFT which yields variable α values and can be used to accurately predict the fluid flow. As this dataset is a soil sample, we generalize the soil- water diffusivity (D_{α}^{R}), Eq. (6) which is derived from the Richards' equation by Richards (1931). This serves as an accurate approach to describe the fluid flow and we use it as the input to solve the GFFT in fitting to the dataset.

4.1.2 El Abd and Milczarek (2004) dataset

This dataset from El Abd and Milczarek (2004) includes two types of building materials: (1) fired brick clay and (2) siliceous brick which they applied dynamic neutron radiography to obtain the experimental data concerning the kinetics of the wetting process. The samples were prepared as bars, air dried and experimentally measured for imbibition (El Abd and Milczarek, 2004). They recorded real time images or radiograms to determine the advancing water content variation in to the medium at different positions or distances as a function of time. We fit the solution of GFFT to the data reported to optimize the α values and validate the approach of GFFT in modeling SI. For both experiments the power-law diffusivity in the form of $D_\alpha(\theta) = C_0\theta^n(\frac{mm^2}{s^\alpha})$ was used as the input to the solution of GFFT with C_0 = 0.075 and n = 1.75 for the fired-brick clay samples and C_0 = 0.98 and n = 8.2 for the siliceous brick samples.

4.1.3 Qin et al. (2022) dataset

We use the Estaillades carbonates stimulation data reported by Qin et al. (2022). They investigated the effect of pore scale heterogeneity by means of direct flow stimulations. The carbonates used exhibits significant pore scale heterogeneity (Qin et al., 2022). And they reported the saturation-time curves for different contact angles (20°,40°,60° and 80°). In our work we show that we can fit the solution of GFFT to find the α values and the imbibition time exponents in each case. Here we generalize Eq. (2b) to use as the input to solve the GFFT. The capillary pressure data for the same rock type from three articles from the literature (Bultreys et al., 2016, Bultreys et al., 2015 and Qin et al., 2022) were used to increase the accuracy of the data. The relative permeabilities were estimated out of the optimized parameters of capillary pressure data fitted to the Van-Genuchten Mualem model by Van Genuchten (1980). These parameters were used as the inputs to generalize and calculate the diffusivity using Eq. (2b) which serves as the input for scaling model and modeling GFFT.

4.1.4 Meng et al. (2022) dataset

Meng et al. (2022) reported experimental and stimulation counter-current SI data using quartz sand packs. They used an irregular shaped quartz sands with a narrow range of particle size distribution. Synthetic brine was used as the wetting phase and air, kerosene. White oil-15, white-oil 32 were used as the non-wetting phases. We generalize Eq. (2b) and calculate the two-phase flow diffusivity to use as the input for the GFFT. Also, we use the capillary pressure data for quartz sand reported by Ghanbarian et al. (2018) and estimate the relative permeabilities for the two phases using the Van-Genuchten Mualem model, which serves as inputs for the calculation of diffusivity. Then we fit the GFFT to the recovery data reported to estimate the α values for each case.

4.2 Fitting the GFFT to the data

In this study, the GFFT is solved to model the SI using a mathematical approach. The partial differential equation, Eq. (4) is reduced to a pair of ordinary differential equations as explained in the theory section. The main input for the GFFT is the diffusivity. The diffusivity can take different forms based on the type of media. We mainly generalize and use the two-phase flow diffusivity, Eq. (2b) and the typical soil water diffusivity Eq. (6). It is important to note that in this work, we generalized the diffusivities introducing α to the equations. The diffusivity is calculated based on the capillary pressure and relative permeability data which serves as the salient properties in describing SI. We estimate the relative permeabilities from the Van-Genuchten Mualem models given below (Ruprecht et al., 2014),

$$k_w = \left(\frac{S_w - S_{wr}}{1 - S_{wr}}\right)\left[1 - \left(1 - \frac{S_w - S_{wr}}{1 - S_{wr}}\right)^{1/m}\right]^{2m} \tag{16}$$

$$k_{nw} = \left(1 - \left(\frac{S_w - S_{wr}}{1 - S_{wr} - S_{nr}}\right)\right)\left(1 - \left(\frac{S_w - S_{wr}}{1 - S_{wr} - S_{nr}}\right)^{1/m}\right)^{2m} \tag{17}$$

where k_w is the relative permeability of the wetting phase, k_{nw} is the relative permeability of the non-wetting phase, S_w is the wetting saturation, S_{wr} is the residual wetting saturation, S_{nr} is the residual non-wetting phase saturation. Parameter m is optimized using the capillary pressure data.

We use the estimated relative permeability data and the capillary pressure data to calculate the diffusivity which we use as the input to solve GFFT. In solving GFFT, we utilize the solve.bvp package of python to solve two ordinary differential equations (Eqs. 10 and 11) as a boundary value problem using the given boundary conditions. The solution allows us to predict the imbibition of a phase to a medium as a function of time.

4.3 Scaling analysis of counter-current SI

To evaluate the GFFT and non-Boltzmann transformation in the SI scaling, we collected data including experimental measurements and numerical stimulations, covering a wide range of porous materials from the literature. We analyzed the experimental SI data reported by Fischer et al. (2008), Zhang et al. (1996), Zhou et al. (2002), Hamon et al. (1986), Bourblaux and Kalaydjian (1990) and Babadagli and Hatiboglu (2007) which includes 25 sandstones, 2 diatomites, and 6 synthetic porous media. We also analyzed numerical stimulation SI data reported by Qin et al. (2022) and Meng et al. (2022) which includes carbonates and quartz sand. To collapse the SI data into a single curve, we normalized the recovery factor or water saturation by its maximum value (Zhang et al., 1996) against the dimensionless time by using the model (Eq. 15) we introduced in this study. We found that the non-Boltzmann transformation (variable α) yielded a better collapse in the SI data than the Boltzmann transformation (α = 1). We compared the scaling of the same dataset by the model introduced by Schmid and Geiger (2012). All the datasets used in this study are briefly described in the following subsections.

4.3.1 Zhang et al. (1996) dataset

Zhang et al. (1996) reported experimental SI data for Berea sandstones. A synthetic reservoir brine and white oil was used as the wetting and non-wetting phase for the imbibition experiments respectively. The cores were prepared with different boundary conditions subjecting to imbibition. The cores we analyzed have boundary conditions of one end open (OEO), two ends open (TEO) and Two ends closed (TEC) subjecting to imbibition. The core samples were oven dried and counter-current imbibition experiments were carried out. We digitized the oil recovery data reported to use in our analysis. Core dimensions and other properties like porosity reported were used in the calculations

4.3.2 Hamon et al. (1986) dataset

Hamon et al. (1986) reported experimental imbibition data of both synthetic porous samples and sandstones. Synthetic porous samples were made of aluminum silicate. Filtered degassed water and purified refined oil was used as the wetting and non-wetting fluids respectively. The samples analyzed in this study were subjected to both ends open, lower face open, core fully immersed in water boundary conditions during the experiments (Hamon et al., 1986). We used the reported fluid rock parameters of cores used in the experiments in the dimensionless calculations.

4.3.3 Zhou et al. (1986) dataset

Zhou et al. (2002) carried imbibition experiments using diatomite samples from Grefco quarry, CA. The samples were prepared into cylindrical cores and subjected to imbibition to determine the fluid displacements mechanisms during counter current SI. The experiments were done for both co-current and counter-current SI and they collected images periodically to record the oil recovery as a function of time. The reported recovery vs imbibition time data were used to calculate the dimensionless time.

4.3.4 Fischer et al. (2006) dataset

Fischer et al. (2008) reported experimental imbibition data for cylindrical Berea sandstones. They rinsed, oven dried the cores for two days and carried out imbibition experiments for different boundary conditions including one end open, radial two ends closed, and all faces open. Refined oil was used as the non-wetting phase and Glycerol mixed with brine used as the wetting-phase in the SI experiments. The oil production as a function of time was measured for the samples.

4.3.5 Bourblaux and Kalaydjian (1990) dataset

Bourblaux and Kalaydjian (1990) reported experimental imbibition data with fine well sorted Triassic sandstone samples from Vosges region France. They cut the samples with a parallel piped shape with rectangular cross sections of 61 x 21 mm and length of 290 mm. They used brine and refined oil as the wetting and non-wetting fluids for the SI experiments. The blocks were subjected to both co-current and counter-current imbibition tests and the oil recovery was measured and reported as a function of time.

4.3.6 Babadagli and Hatiboglu (2007) dataset

Babadagli and Hatiboglu (2007) also reported imbibition data for Berea sandstones, which were prepared as cylindrical core plugs having three different diameters of length 2, 4 and 6 inches. The boundary condition used was one side open to imbibition and the experiments were performed by positioning the cores horizontally and vertically. They performed air-water imbibition experiments and water with temperatures 90 and 20 degrees were used to investigate the effect of temperature on imbibition. The gas recovery was reported as a function of time for the experiments.

A values needed to calculate the dimensionless time for above datasets were reported by Schmid and Geiger (2012). Other salient properties of the SI measurements used to evaluate the proposed scaling analysis in this study, Eq. (15), are reported in Table 1.

Table 1. Physical properties of the data used in scaling, α values and data sources

Reference	Sample	L_c (cm)	k (mD)	ϕ (-)	μ_w (Pa.s)	μ_{nw} (Pa.s)	S_i (-)	A (m/$\sqrt{s}$)	α (-)
Zhang et al. (1996)	BA31	13.87	907.1	0.214	9.67×10^{-4}	0.03782	0	4.65×10^{-6}	1.18
	BC13	4.99	503.6	0.209	9.67×10^{-4}	0.03782	0	7.05×10^{-6}	1.18
	BC21	6.09	481.9	0.213	9.67×10^{-4}	0.00398	0	1.25×10^{-5}	0.95
	BC22	5.68	496.8	0.208	9.67×10^{-4}	0.15630	0	4.46×10^{-6}	1.20
	BD14	1.35	518.9	0.218	9.67×10^{-4}	0.03782	0	7.34×10^{-6}	1.12
	BD15	1.35	523.8	0.214	9.67×10^{-4}	0.00398	0	1.28×10^{-5}	1.14
	BD18	1.35	509.7	0.218	9.67×10^{-4}	0.15630	0	4.65×10^{-6}	1.13
Haman and Vidal (1986)	A10	9.7	4000	0.472	0.001	0.0115	0.189	3.36×10^{-5}	1.07
	A10-20	19.7	3430	0.453	0.001	0.0115	0.187	3.10×10^{-5}	1.07
	A10-30	30.0	3830	0.453	0.001	0.0115	0.151	3.18×10^{-5}	1.09
	A10-40	40.0	3550	0.478	0.001	0.0115	0.172	3.33×10^{-5}	1.07
	A10-85	84.7	3000	0.478	0.001	0.0115	0.164	3.13×10^{-5}	0.90
	A10VI-20	19.8	3200	0.456	0.001	0.0115	0.164	3.17×10^{-5}	1.21
	A10X-20	20.0	2300	0.458	0.001	0.0115	0.132	2.92×10^{-5}	1.54
Zhou et al. (2002)	Core-4	9.5	2.5	0.78	0.001	8.4×10^{-4}	0	2.72×10^{-5}	1.00
	Core-5	9.5	6.0	0.68	0.001	8.4×10^{-4}	0	2.86×10^{-5}	1.03
Fischer et al. (2006)	EV6-22	7.18	109.2	0.18	0.495	0.0039	0	4.29×10^{-7}	1.01
	EV6-18	7.62	140.0	0.181	0.001	0.063	0	3.74×10^{-6}	1.04
	EV6-21	7.7	107.3	0.187	0.0278	0.0039	0	1.86×10^{-6}	0.99
	EV6-13	7.75	113.2	0.187	0.001	0.0039	0	7.48×10^{-6}	1.00
	EV6-14	7.66	127.2	0.178	0.0041	0.0039	0	4.45×10^{-6}	1.00
	EV6-20	7.52	132.9	0.181	0.0041	0.0633	0	2.45×10^{-6}	1.03
	EV6-16	7.78	136.8	0.181	0.0278	0.0633	0	1.36×10^{-6}	1.00
	EV6-23	7.36	132.1	0.179	0.0977	0.0039	0	9.92×10^{-7}	1.00
	EV6-15	7.3	107.0	0.183	0.4946	0.0633	0	3.93×10^{-7}	0.99
	EV6-17	7.54	128.1	0.19	0.0977	0.0633	0	8.59×10^{-7}	1.00
Bourboaux and Kalaydjian (1990)	GVB-3	29.0	124.0	0.233	0.0012	0.0015	0.4	1.24×10^{-5}	1.02
	GVB-4	14.5	118.0	0.233	0.0012	0.0015	0.411	9.67×10^{-6}	1.03
Babadagli and Hatiboglu (2007)	F-11	10.16	500.0	0.21	0.001	1.8×10^{-5}	0	2.75×10^{-5}	1.01
	F-12	15.24	500.0	0.21	0.001	1.8×10^{-5}	0	2.81×10^{-5}	1.06
	F-14	10.16	500.0	0.21	0.001	1.8×10^{-5}	0	1.95×10^{-5}	1.04
	F-16	5.08	500.0	0.21	0.001	1.8×10^{-5}	0	2.29×10^{-5}	0.88
	F-17	10.16	500.0	0.21	0.001	1.8×10^{-5}	0	1.60×10^{-5}	1.01
	F-18	15.24	500.0	0.21	0.001	1.8×10^{-5}	0	2.07×10^{-5}	0.99

4.3.7 Qin et al. (2022) dataset

We demonstrate that the saturation vs time numerical stimulation SI data for Estaillades carbonates reported by Qin et al. (2022) can be scaled to fall onto a single curve by the model we developed using the GFFT approach. We show that the α values we used to scale or collapse the curves into a single curve relate to the α values coming out of the fits of the GFFT to the data in most cases. In scaling this dataset, we use and generalize the two-phase flow diffusivity (D_{α}^{F}), Eq. (2b) and we use the capillary pressure data reported by Bultreys et al. (2015), Bultreys et al. (2016) and Qin et al. (2022) to estimate relative permeabilities and calculate the rest of parameters we use in our scaling model.

4.3.8 Meng et al. (2022) dataset

Apart from modeling the reported data using GFFT as stated in section 4.1.4, we scale the oil recovery SI data using our model (Eq. 15) to show that we can collapse the data on to a single curve. In the results we show that the variable α values which makes the data collapse depends on the viscosity ratio. Again, for this dataset, we use the capillary pressure data by Ghanbarian et al. (2018) to estimate relative permeabilities and calculate generalized two-phase flow diffusivity (D_{α}^{F}), Eq. (2b) which is needed to calculate the fractional flow function and constant A (see Eqs. 23 and 24 in Mcwhorter and Sunada (1990) that we use in our scaling model.

4.4 SI in individual rough-wall fractures

As a part of this study, we also investigated the SI in rough-wall fractures. The experimental data used in this study are Perfect et al. (2020) who measured the SI on three Crossville sandstones and three Mancos shales. The porosity, fracture aperture width and fracture surface fractal dimensions were determined during the experiments. Perfect et al. (2020) reported average porosity equal to 5.85 and 5.59%, average aperture size equal to 92 and 104 μm

respectively for the Crossville sandstones and Mancos shales. In both rock type, they found the average surface fractal dimension equal to 2.16. The SI experiments were carried out following dynamic neutron radiography technique using oven dried cores subjected to imbibition. The cores were imaged during the experiments, and they reported heights of wetting front vs time taken for imbibition for the experiments (see their Figure 4). In this study, we fit the non-Boltzmann equation, $x = \lambda t^{\frac{\alpha}{2}}$, to the height-time data to optimize the exponent α.

Chapter 5 - Results and Discussion

In this section, we first present the results of modeling the counter-current SI via the GFFT, Eq. (4), and discuss them in detail. We then demonstrate how the generalized approach of Schmid and Geiger (2012) result in a much more accurate collapse of the SI data.

5.1 Modeling counter-current SI via the GFFT

5.1.1 Ferguson and Gardner (1963) dataset

We fitted the GFFT to the water content (θ) vs time data reported by Ferguson and Gardner (1963). In this study, we convert the water content to water saturation using porosity to keep the consistency. The solution of GFFT fits well with all the experiments (Distance from the water source – 3.5, 7.5, 11.5, 15.5, 19.5,21.5, 23.5, and 27.5 cm) showing the applicability of the GFFT in predicting and modeling SI. The fits of GFFT yielded variable α values ranging from 0.85 to 0.94 which shows that the fluid flow in the medium does not follow the traditional Boltzmann approach where α is fixed at 1 and follows the generalized non-Boltzmann approach. The fit of the solution of GFFT to four experiments from Ferguson and Gardner (1963) are shown in Fig. 1. As can be seen, the GFFT fit the data very well. We found α = 0.93, 0.90, 0.93 and 0.93, with an average value of 0.921, for $x = 3.5$, 7.5, 15.5 and 27.5 cm, respectively.

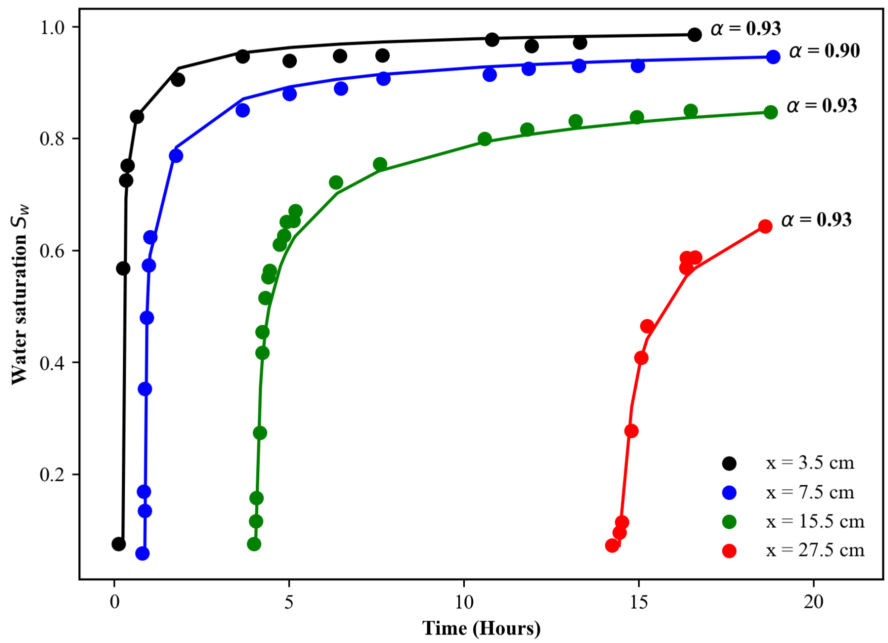

Figure 1. Four experiments reported by Ferguson and Gardner (1963), shown by filled circles, and the fitted GFFT, Eq. (4), shown by solid lines. The optimized exponents are reported next to each experiment.

The average value of $\alpha = 0.921$ determined from the experiments shown in Fig. 1 corresponding to $x = 3.5$, 7.5, 15.5 and 27.5 cm is very close to 0.91 reported by Pachepsky et al. (2003) who solve Eq. (4) using a different approach based on the generalized Richards' equation (see Eq. (6) in Pachepsky et al. (2003)). Most importantly, they show that the soil solution shows non-Boltzmann scaling instead of Boltzmann scaling. It is important to know that Pachepsky et al. (2003) reported an average α value of 0.91 based on the collapsing of four experiments mentioned above. We fitted the GFFT to the four experiments individually, found individual α values and obtained a closer average of 0.921, which shows the applicability of our approach in explaining the fluid flow in soil media.

5.1.2 El Abd and Milczarek (2004) dataset

We present the fit of the solution of the GFFT to the fired-brick clay and siliceous brick experiments from El Abd and Milczarek (2004) in Fig. 2. As can be observed, the GFFT characterized the wetting fronts reasonably well in most cases.

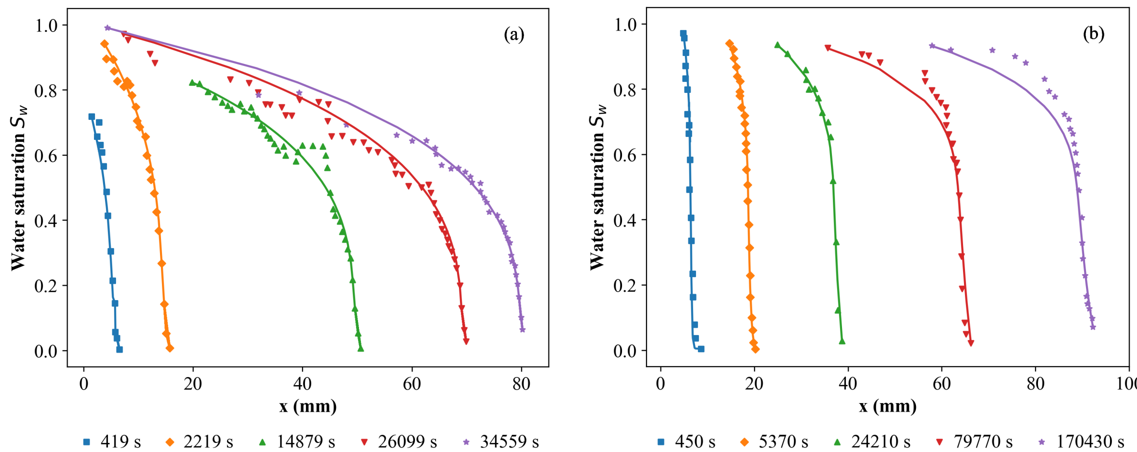

Figure 2. Experiments, shown by filled symbols, from El Abd and Milczarek (2004) for (a) the fired-clay brick and (b) siliceous brick samples. The solid lines represent the fit of the solution of the GFFT, Eq. (4).

By fitting the solution of the GFFT, Eq. (4), to each experiment, we optimized the non-Boltzmann scaling exponent and found α = 1.07. 1.07, 1.21, 1.14 and 1.14 for t = 419, 2219, 14879, 26099 and 34559 seconds, respectively, for the fired-clay brick sample. The average value of 1.13 is near to 1.24 reported by Sun et al. (2013) who used one single exponent to characterize all the experiments. For the siliceous brick sample, we found smaller α values compared to the fired-clay brick sample. More specifically, our fitting analysis resulted in α = 0.85. 0.85, 0.90, 0.93 and 0.90 for t = 450, 5370, 24210, 79770 and 170430 s, respectively, with an average value of 0.89 that is very close to 0.86 reported by Sun et al. (2013).

5.1.3 Qin et al. (2022) dataset

We present the solution of GFFT, fitting to the estaillades carbonates numerical stimulation SI data reported by Qin et al. (2022) in Fig. 3. The closer fits show that, the GFFT approach predicts the wetting fronts accurately.

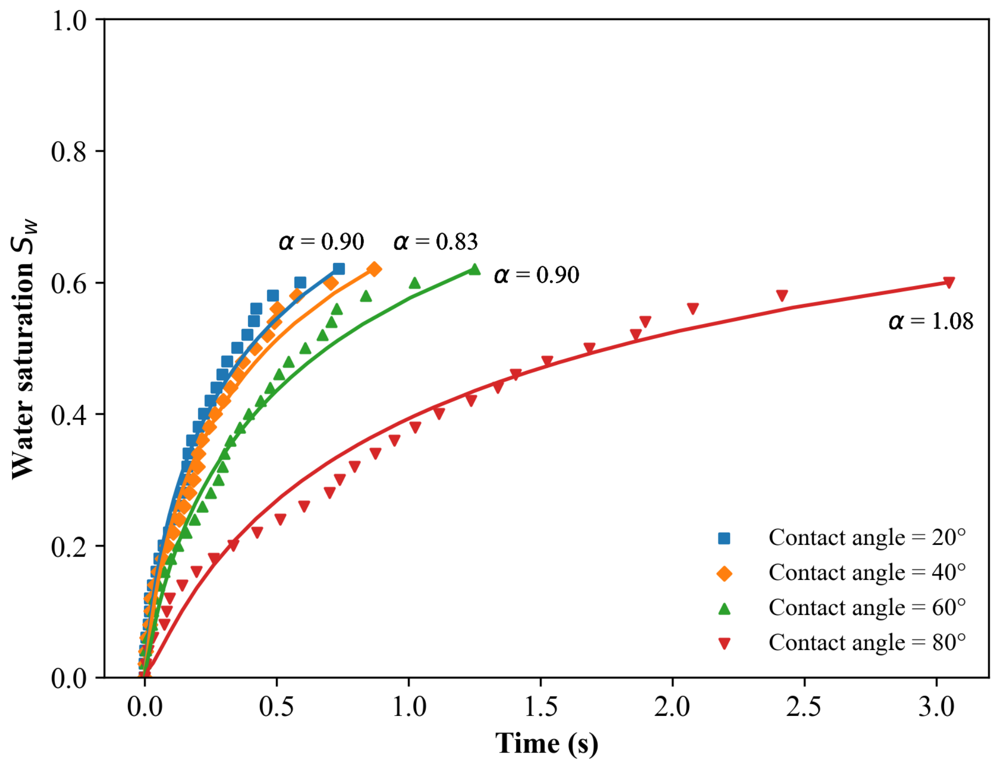

Figure 3. Fitting of GFFT to the imbibition curves of Estaillades carbonates dataset reported by Qin et al. (2022). The lines indicate the fits, and the points indicates the data for each contact angle. The resulting α values are shown next to each case.

Results of fitting the solution of the GFFT, Eq. (4), for this dataset are shown in Fig. 3. We found α = 0.90, 0.83, 0.90 and 1.08 respectively for contact angles 20°, 40°, 60° and 80°. Results clearly show the dependency of α on wettability similar to the results of Bakhshian et al. (2020) who conducted color gradient lattice-Boltzmann simulations in water- and intermediate-wet rock images of a Tuscaloosa sandstone and reported that wettability was a major factor caused scaling exponents different from 0.5 in the Boltzmann transformation (where α = 1).

Generally speaking, we found an increasing trend between the non-Boltzmann scaling exponent and contact angle. However, further investigations are required to study the effect of wettability on the exponent α more comprehensively using a wider range of contact angles as well as in heterogeneously wet media.

The α values less or greater than 1 found in this study clearly demonstrate the application of the GFFT, Eq. (4), to both experimental measurements and numerical simulations. More specifically, we found that the non-Boltzmann scaling exponent depends on the heterogeneity in the pore space but also fluid-solid properties, such as contact angle.

5.1.4 Meng et al. (2022) dataset

We present the results and fits of GFFT to the experimental and stimulation SI data reported by Meng et al. (2022) for quartz sand packs. The fits are presented in Fig. 4 and the close fits show that GFFT reasonably characterized the wetting fronts.

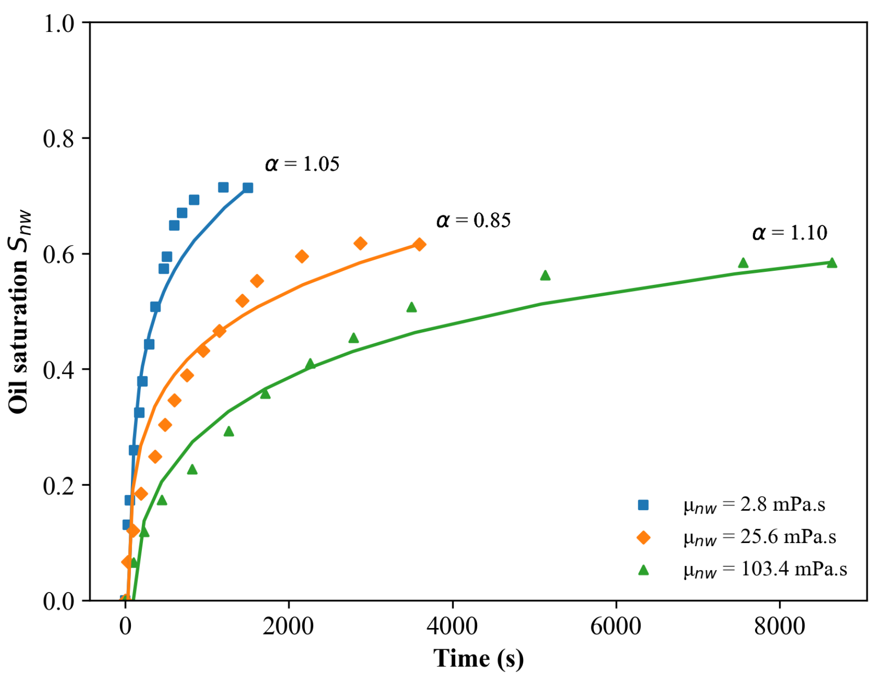

Figure 4. Fitting of GFFT to the imbibition curves of quartz sand packs dataset reported by Meng et al. (2022). The lines indicate the fits, and the points indicates the data for different dynamic non-wetting phase viscosities. The resulting α values are shown next to each case.

Based on the fits, we found α = 1.05, 0.85, and 1.10 respectively for dynamic non-wetting viscosities of 2.8, 25.6 and 103.4 mPa.s for non-wetting fluids kerosene, white oil-15 and white oil-32 respectively. The results clearly show the dependency of α on dynamic viscosity of the non-wetting phase. Diao et al. (2021) also reported that mixed wettability or different viscosity ratios affect SI in heterogenous porous media by numerical stimulations using quasi-3D color-gradient lattice-Boltzmann method by Liu et al. (2021). Based on the relationship between wetting saturation and imbibition time they show that the scaling exponent deviates from the Lucas-Washburn exponent. This is further justified by our results, using the GFFT in characterizing SI which shows that the scaling exponents different from 0.5 in Boltzmann transformation (where α = 1). However, we used estimated capillary pressure data and relative permeability data in our work analyzing this dataset. We strongly suggest that using experimented data for the inputs and use GFFT approach could result more accurate results in terms of characterizing SI.

5.2 Scaling SI data across various porous media

The results of scaling analysis are shown in Fig. 5. Fig. 5a exhibits the unscaled SI data indicating diversity and scatter in the measurements for a wide range of porous media types, experimental conditions, and water-air and water-oil mixtures. In Fig. 5b, we show the scaled SI data using the Schmid and Geiger (2012) approach. As can be observed, although most data fall onto a curve, there still exist scatters. It is important to note that, Fig. 5b here in this work differs to a certain extent from Fig. 4b in Schmid and Geiger (2012) possibly because we collected SI recovery data more extensively from the same literature Schmid and Geiger (2012) used and they have selectively chosen certain SI data in visualizations. Fig. 5c demonstrates the results of our proposed scaling based on the GFFT and non-Boltzmann transformation. As can be seen, with reasonable α values ranged from 0.88 to 1.54 (Table 1), the scaled SI data nearly collapsed onto a single universal curve. This confirms the practical application of the proposed scaling analysis. One, however, should note that to scale the SI data reported here, we used the A values and other parameters like porosity (ϕ) and characteristic length (L_c) reported by Schmid and Geiger (2012) in this work. And they used estimated capillary pressure and relative permeability data to calculate diffusivity based on the analytical approach of Mcwhorter and Sunada (1990). We strongly argue that if one use experimental capillary pressure and relative permeability data as inputs, the proposed scaling analysis can be used to scale SI much accurately.

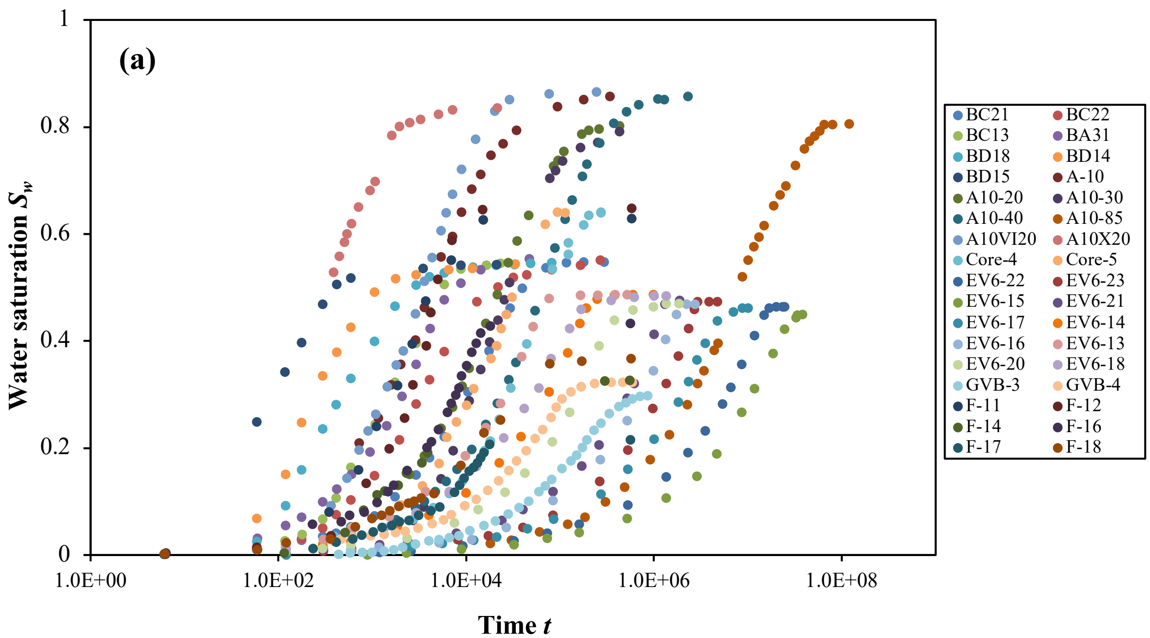

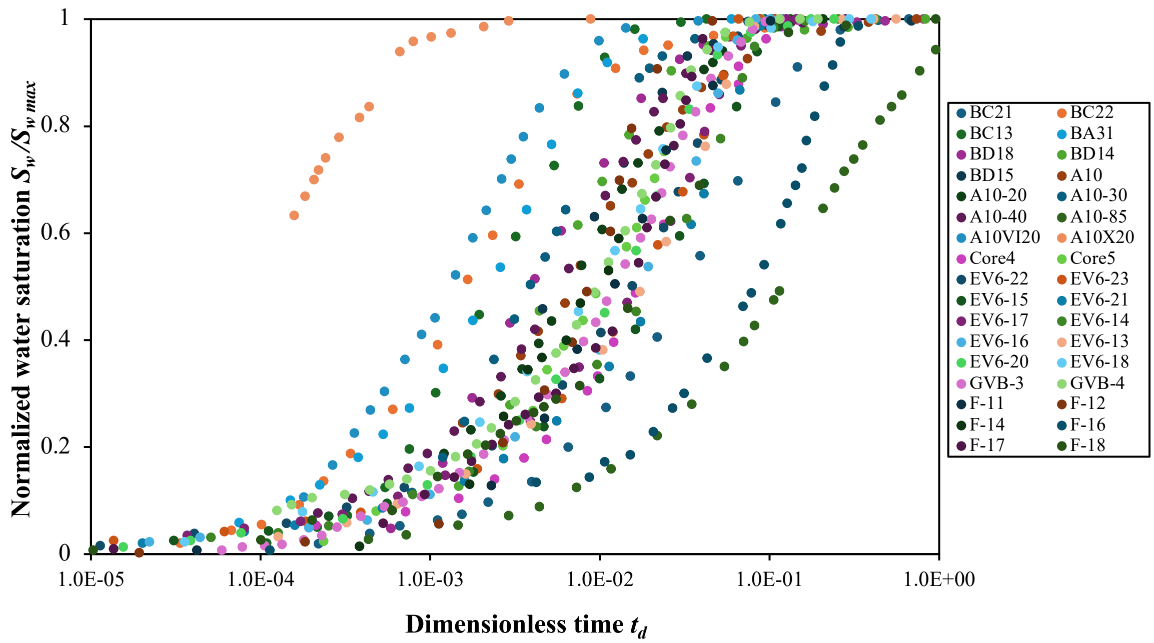

Normalized water saturation $S_w/S_{w\,max}$
Dimensionless time t_d
0
0.2
0.4
0.6
0.8
1
1.0E-05
1.0E-04
1.0E-03
1.0E-02
1.0E-01
1.0E+00
BC21
BC22
BC13
BA31
BD18
BD14
BD15
A10
A10-20
A10-30
A10-40
A10-85
A10VI20
A10X20
Core4
Core5
EV6-22
EV6-23
EV6-15
EV6-21
EV6-17
EV6-14
EV6-16
EV6-13
EV6-20
EV6-18
GVB-3
GVB-4
F-11
F-12
F-14
F-16
F-17
F-18

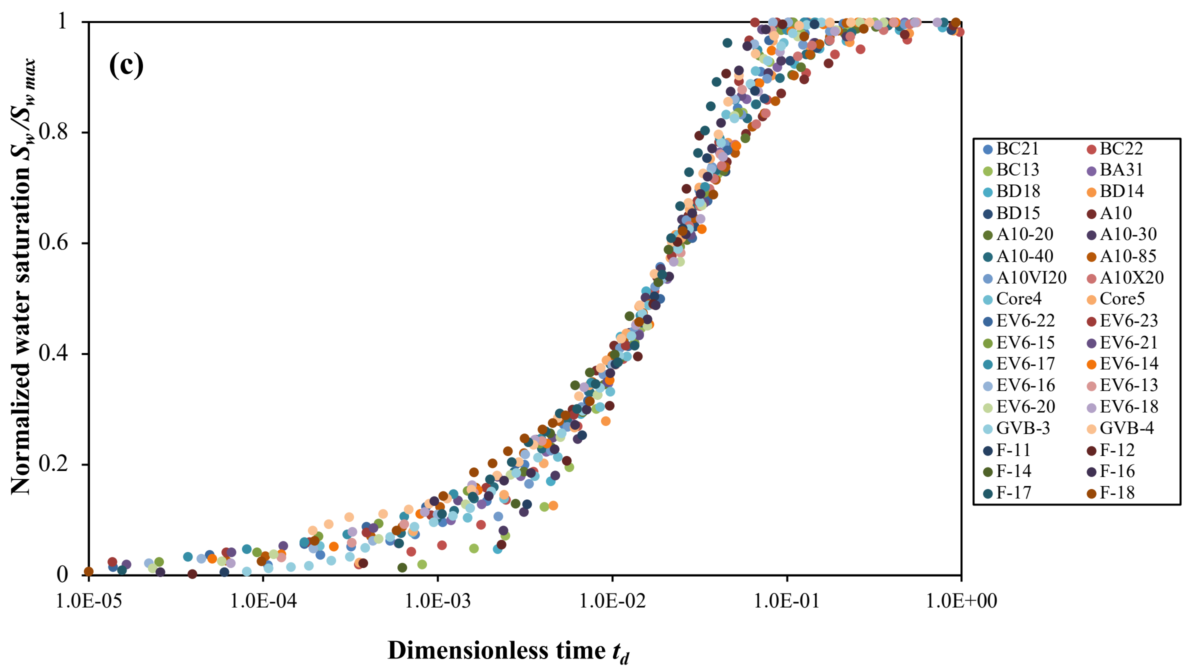

(c)
Normalized water saturation $S_w/S_{w\,max}$
Dimensionless time t_d
0
0.2
0.4
0.6
0.8
1
1.0E-05
1.0E-04
1.0E-03
1.0E-02
1.0E-01
1.0E+00
BC21
BC22
BC13
BA31
BD18
BD14
BD15
A10
A10-20
A10-30
A10-40
A10-85
A10VI20
A10X20
Core4
Core5
EV6-22
EV6-23
EV6-15
EV6-21
EV6-17
EV6-14
EV6-16
EV6-13
EV6-20
EV6-18
GVB-3
GVB-4
F-11
F-12
F-14
F-16
F-17
F-18

Figure 5. (a) Water saturation versus time collected from the literature. (b) Normalized water saturation against dimensionless time based on scaling analysis of Schmid and Geiger (2012). (c) Normalized water saturation against dimensionless time, Eq. (15), proposed in this study.

We also applied the proposed scaling approach to four SI sets of simulations on an Estaillades carbonate sample reported by Qin et al. (2022) and experimental and stimulation SI data on quartz sand pack samples by Meng et al. (2022). And we compared the scaling with the model introduced by Schmid and Geiger (2012) which acts as a special case of our model where α = 1. Fig. 6 compares the scaling of the imbibition curves with Boltzmann approach and non-Boltzmann approach for the SI data reported by Qin et al. (2022) and Meng et al. (2022). The results showed that the data is not collapsed well with α fixing at 1, or in other words using the previous approach, but it gave a decent collapse when we used our approach with varying α values. Also, in some cases we were able to find closer α values to the values we found with the fitting of GFFT to the imbibition curves. This result provides solid evidence that using the GFFT in combination with the non-Boltzmann transformation in modeling two phase flow and scaling SI predicts the flow behavior and captures the heterogeneity accurately than the classical Richards' equation and Boltzmann transformation, which restricts the flexibility of the imbibition exponent. Also, this observation provides solid evidence that α value depends on the contact angle and the dynamic viscosity of the fluids used.

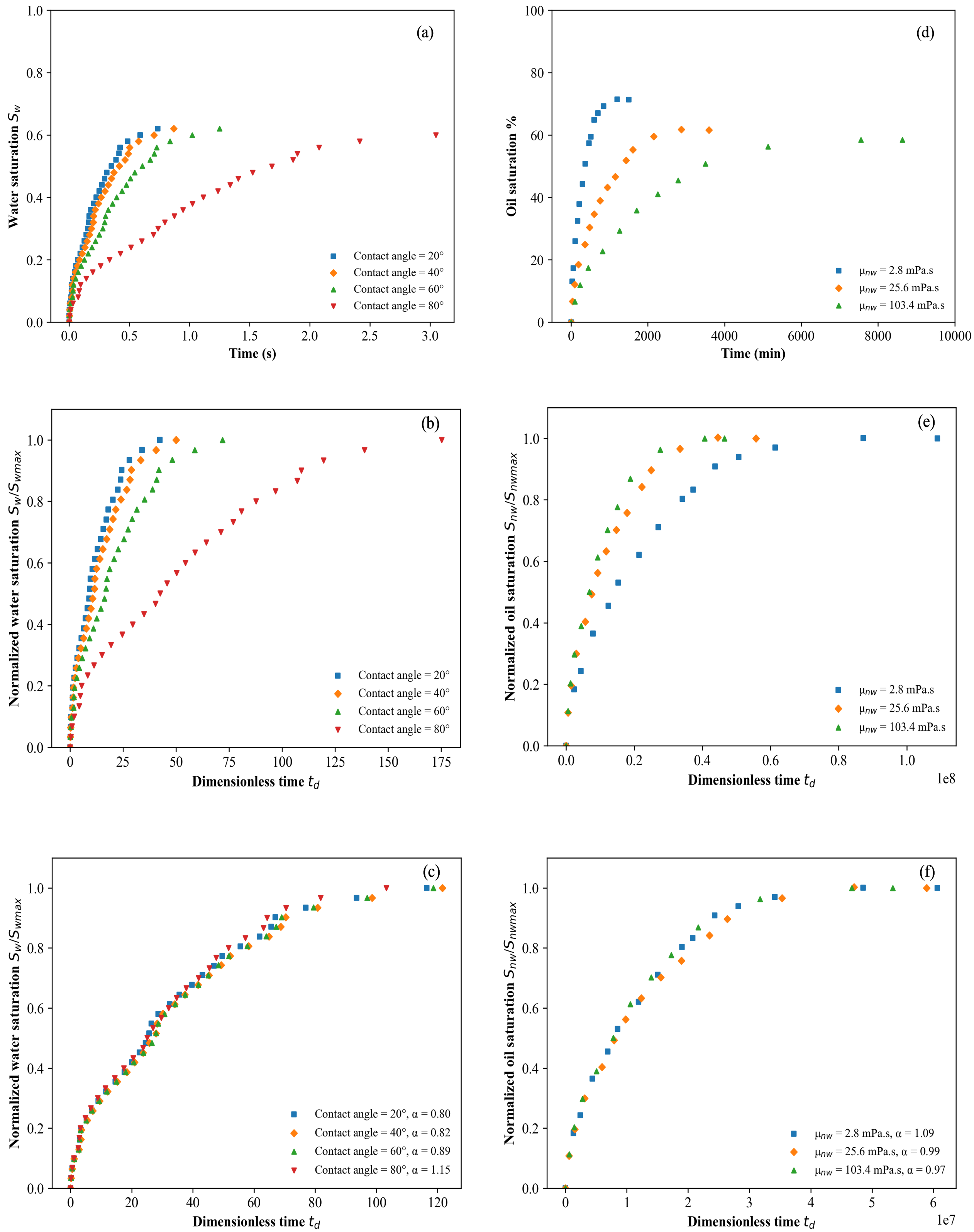

(a)
Water saturation S_w
Time (s)
Contact angle = 20°
Contact angle = 40°
Contact angle = 60°
Contact angle = 80°
(d)
Oil saturation %
Time (min)
μ_{nw} = 2.8 mPa.s
μ_{nw} = 25.6 mPa.s
μ_{nw} = 103.4 mPa.s
(b)
Normalized water saturation S_w/S_{wmax}
Dimensionless time t_d
Contact angle = 20°
Contact angle = 40°
Contact angle = 60°
Contact angle = 80°
(e)
Normalized oil saturation S_{nw}/S_{nwmax}
Dimensionless time t_d
1e8
μ_{nw} = 2.8 mPa.s
μ_{nw} = 25.6 mPa.s
μ_{nw} = 103.4 mPa.s
(c)
Normalized water saturation S_w/S_{wmax}
Dimensionless time t_d
Contact angle = 20°, α = 0.80
Contact angle = 40°, α = 0.82
Contact angle = 60°, α = 0.89
Contact angle = 80°, α = 1.15
(f)
Normalized oil saturation S_{nw}/S_{nwmax}
Dimensionless time t_d
1e7
μ_{nw} = 2.8 mPa.s, α = 1.09
μ_{nw} = 25.6 mPa.s, α = 0.99
μ_{nw} = 103.4 mPa.s, α = 0.97

Figure 6. Scaling of SI data reported by Qin et al. (2022) and Meng et al. (2022) using two approaches. (a) Water saturation versus time collected from Qin et al. (2022). (b) Normalized water saturation against dimensionless time based on scaling analysis of Schmid and Geiger (2012) for data reported in (a). (c) Normalized water saturation against dimensionless time, based on Eq. (15), proposed in this study for data reported in (a). (d) Water saturation versus time collected from Meng et al. (2022). (b) Normalized water saturation against dimensionless time based on scaling analysis of Schmid and Geiger (2012) for data reported in (d). (c) Normalized water saturation against dimensionless time, based on Eq. (15), proposed in this study for data reported in (d).

Based on Fig. 6c and 6f, it is evident that, the non-Boltzmann approach used in this study collapses SI data into a universal curve with less scattering than one of the previous models used by Schmid and Geiger (2012). The α values which yields a good collapse of the curves are reported in the legend of Fig. 6c and 6f.

5.3 Non-Boltzmann scaling in individual rough-wall fractures

We also investigated the variation of α in rough-wall fractures during imbibition by fitting the non-Boltzmann transformation equation, $x = \lambda t^{\frac{\alpha}{2}}$ to the wetting front height against the imbibition time data reported by Perfect et al. (2020). The fits shown in Fig. 7 are reasonable with $R^2 > 0.95$. We found $\alpha = 1.15$, 1.24 and 1.07, with an average value of 1.15, for the three Crossville sandstones. And, for the three Mancos shale, we found $\alpha = 0.87$, 0.92 and 0.98, with an average value of 0.92. Results showed exponents different from 0.5 meaning that the Boltzmann scaling does not necessarily scale time and height in rough-wall fractures. Although both sandstone and shale samples studied here had the same surface fractal dimension (equal to 2.16), the average α value for the Crossville sandstone was different from that for the Mancos shale. This indicates the trivial impact of surface roughness on the non-Boltzmann scaling exponent α. Interestingly, we found the average α = 1.15 for the Crossville sandstone samples with an average aperture of 92 μm, while average α = 0.92 for the Mancos shale samples with an average aperture of 104 μm, which indicate an inverse trend between the exponent α and the average aperture size. Recently, Ning et al. (2022) investigated the effect of the presence of micro-fractures within rock matrix and found exponents different from 0.5. They argued that the micro-fracture orientation (e.g., parallel or transverse) caused deviation from the Boltzmann scaling. Nonetheless, further investigations using a broader range of fractures with various roughness and aperture sizes are still needed to study how the exponent α may vary within individual rough-wall fractures.

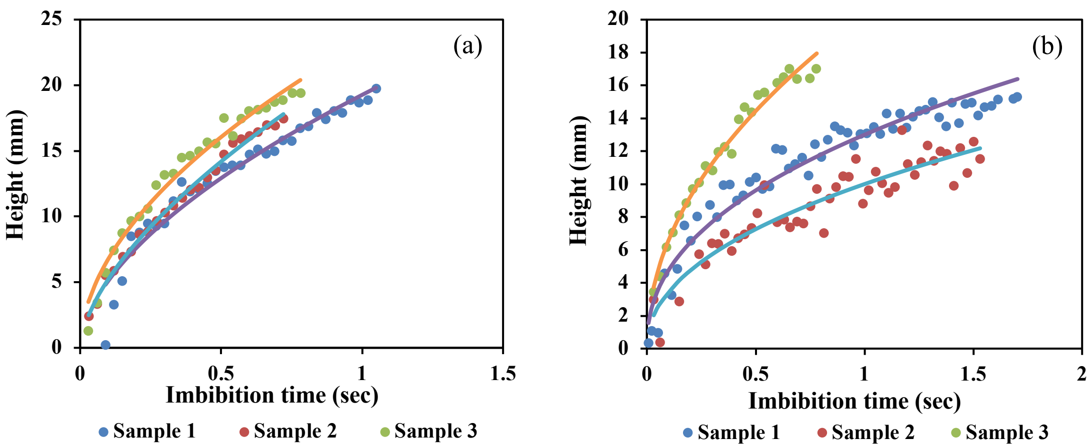

Figure 7. Experiments reported by Perfect et al. (2020), shown by filled circles, and the fitted non-Boltzmann equation, shown by solid lines for (a) Crossville sandstones and (b) Mancos shale.

Chapter 6 - Conclusion

Modeling and scaling counter-current SI have been a long-standing challenge in the past several decades due to its practical applications, such as CO_2 sequestration. Although various SI models were developed in the literature, they have some limitations. In this study, we generalized fractional flow theory using concepts of time fractional derivatives and non-Boltzmann transformation to model the counter-current SI. We validated the new scaling model by analyzing more than 30 samples including sandstones, diatomite, synthetic porous media and carbonates with varying porosities, initial water contents, dynamic viscosities to show the general applicability of the model across various porous media. The scaled data falls on to a universal curve (Fig. 5 and 6) strongly indicating the suitability of the model to scale SI data. We suggest using the measured experimental capillary hydraulic properties, like capillary pressure and relative permeabilities to further improve scaling. It is important to note that, capturing these properties is vital to accurately scale the data using the model to calculate t_d.

In this work, most importantly we show that use of traditional Richards' equation which implies that the wetting front in a medium follows Boltzmann scaling with the travel distance proportional to square root of time is not applicable and accurate for most of the porous media and soil. Instead, in this work we emphasize and prove that use of GFFT captures the fractal nature of the heterogenous porous media and unsaturated soil. The solution of GFFT shows the non-Boltzmann scaling and the time exponent varying around 0.5. We have fitted the solution of GFFT to several applications or datasets from the literature and calculated the α values and shown that the time exponent varies significantly from 0.5.

Also, we show that the variation of α value can be attributed to the contact angle. In Fig 6, the water content curves with 4 contact angles collapse on to a single curve with varying α values.

We show that the obtained α values are close with the fitting of GFFT as well. However, the effect of contact angle on α should be further studied and investigated. We show that, the α value also depends on the viscosity ratios as we predicted the fluid fronts using the GFFT approach and yielding variable α values. It is evident that, GFFT approach supports the previous work on deviation of the imbibition time exponent from Boltzmann transformation (Hu et al., 2012; Kelly et al., 2015; Ning et al., 2022; Diao et al., 2021) which characterized deviation of the imbibition exponent (In this work, we refer to the α value in the imbibition exponent) based on pore connectivity, pore structure, fracture networks inside porous media and wettability. This work serves as a foundation to investigate the relationship of α with the contact angle, viscosity ratio, lithologies, and pore structure from one sample to another. Also, it is important note that the GFFT approach is extremely sensitive to the diffusivity function used as an input. Diffusivity depends on the primary inputs like capillary pressure and relative permeability and the use of experimental data for these inputs are highly recommended to keep the accuracy and minimize errors in the outputs. Using this new approach, we expect to more accurately predict the rate and amount of fluid that can spontaneously imbibe into a porous medium if characteristics such as porosity, permeability, initial and maximum saturations, viscosity, and wettability are known.

Notation

A scaling constant

α non-Boltzmann variable in the imbibition exponent

S_w water saturation

t time

f fractional flow function for viscous flow

x distance

D Two-phase flow diffusivity

P_c Capillary pressure

ϕ porosity

q_t Total flux

q_w Wetting phase flux

q_{nw} Non-wetting phase flux

λ Lambda

D_{α} Fractional diffusivity

t^{α} Fractional time

θ Water content

S_i Initial water saturation

S_0 Final water saturation

S_{wmax} Maximum water saturation

V_b Bulk volume of the sample

L_c Characteristic length

a_i Area of the open face

l_{ai} Distance imbibition front travels towards no flow boundary

t_d	Dimensionless time
Q_w	Cumulative imbibition
k	permeability
μ_w	Dynamic Viscosity of the wetting phase
μ_{nw}	Dynamic Viscosity of the non-wetting phase
k_w	Relative permeability of the wetting phase
k_{nw}	Relative permeability of the non-wetting phase

References

Abd, A. S., Elhafyan, E., Siddiqui, A. R., Alnoush, W., Blunt, M. J., & Alyafei, N. (2019). A review of the phenomenon of counter-current spontaneous imbibition: Analysis and data interpretation. *Journal of Petroleum Science and Engineering*, *180*, 456–470.

Babadagli, T., & Hatiboglu, C. U. (2007). Analysis of counter-current gas-water capillary imbibition transfer at different temperatures. *Journal of Petroleum Science and Engineering*, *55*(3–4), 277–293.

Bakhshian, S., Murakami, M., Hosseini, S. A., & Kang, Q. (2020). Scaling of imbibition front dynamics in heterogeneous porous media. *Geophysical Research Letters*, *47*(e2020GL087914).

Behbahani, H. S., Di Donato, G., & Blunt, M. J. (2006). Simulation of counter-current imbibition in water-wet fractured reservoirs. *Journal of Petroleum Science and Engineering*, *50*(1), 21–39.

Bourblaux, B. J., & Kalaydjian, F. J. (1990). Experimental Study of Cocurrent and Countercurrent Flows in Natural Porous Media. *SPE Res Eng*, *5*, 361–368.

Buckley, S. E., & Leverett, M. (1942). Mechanism of fluid displacement in sands. *Transactions of the AIME*, *146*(1), 107–116.

Bultreys, T., Stappen, J. V., Kock, T. D., Boever, W. D., Boone, M. A., Hoorebeke, L. V., & Cnudde, V. (2016). Investigating the relative permeability behavior of microporosity-rich carbonates and tight sandstones with multi-scale pore network models. *Journal of Geophysical Research: Solid Earth*, *121*(11), 7929–7945.

Bultreys, T., Van Hoorebeke, L., & Cnudde, V. (2015). Multi-scale, micro-computed tomography-based pore network models to simulate drainage in heterogeneous rocks. *Advances in Water Resources*, *78*, 36–49.

Cai, J., Chen, Y., Liu, Y., Li, S., & Sun, C. (2022). Capillary imbibition and flow of wetting liquid in irregular capillaries: A 100-year review. *Advances in Colloid and Interface Science*, *304*(102654).

Cai, J., Perfect, E., Cheng, C. L., & Hu, X. (2014). Generalized modeling of spontaneous imbibition based on Hagen–Poiseuille flow in tortuous capillaries with variably shaped apertures. *Langmuir*, *30*(18), 5142–5151.

Cai, S., Zhang, L., Kang, L., Yang, Y., Jing, W., Zhang, L., Xu, C., Sun, H., & Sajjadi, M. (2021). Spontaneous imbibition in a fractal network model with different wettabilities. *Water (Switzerland)*, *13*(17), 2370.

Deng, L., & Pan, Y. (2021). Application of physics-informed neural networks for self-similar and transient solutions of spontaneous imbibition. *Journal of Petroleum Science and Engineering*, *203*(108644).

Diao, Z., Li, S., Liu, W., Liu, H., & Xia, Q. (2021). Numerical study of the effect of tortuosity and mixed wettability on spontaneous imbibition in heterogeneous porous media. *Capillarity*, *4*(3), 50–62.

El Abd, A. E. G., & Milczarek, J. J. (2004). Neutron radiography study of water absorption in porous building materials: Anomalous diffusion analysis. *Journal of Physics D: Applied Physics*, *37*(16), 2305–2313.

Ferguson, H., & Gardner, W. H. (1963). Diffusion Theory Applied to Water Flow Data Obtained Using Gamma Ray Absorption. *Soil Science Society of America Journal*, *27*(3), 243–246.

Fischer, H., Wo, S., & Morrow, N. R. (2008). Modeling the effect of viscosity ratio on Spontaneous Imbibition. *SPE Reservoir Evaluation & Engineering*, *11*(03), 577–589.

Gao, Z., & Hu, Q. (2016). Wettability of Mississippian Barnett Shale samples at different depths: Investigations from directional spontaneous imbibition. *Aapg Bulletin*, *100*(1), 101–114.

Gao, Z., & Hu, Q. (2023). Assessment of Shale Wettability from Spontaneous Imbibition Experiments. In *Physics of Fluid Flow and Transport in Unconventional Reservoir Rocks* (pp. 177–207).

Ghanbarian, B., Hamamoto, S., Kawamoto, K., Sakaki, T., Moldrup, P., Nishimura, T., & Komatsu, T. (2018). Saturation-dependent gas transport in sand packs: Experiments and theoretical applications. *Advances in Water Resources*, *122*, 139–147.

Gong, J., & Rossen, W. R. (2018). Characteristic fracture spacing in primary and secondary recovery for naturally fractured reservoirs. *Fuel*, *223*, 470–485.

Hamon, G., Aquitaine, E., & Vidal, J. (1986). Scaling-Up the Capillary Imbibition Process From Laboratory Experiments on Homogeneous and Heterogeneous Samples. *SPE Europec Featured at EAGE Conference and Exhibition*, *15852*.

Hu, M. Q., Persoff, P., & Wang, J. S. (2001). Laboratory measurement of water imbibition into low-permeability welded tuff. *Journal of Hydrology*, *242*(1–2), 64–78.

Hu, Q., Ewing, R. P., & Dultz, S. (2012). Low pore connectivity in natural rock. *Journal of Contaminant Hydrology*, *133*, 76–83.

Kelly, S. A. (2015). *Using nanofluidics and microscopy to study unconventional pore-scale transport phenomena*.

Kelly, S., Balhoff, M. T., & Torres-Verdín, C. (2015). Quantification of bulk solution limits for liquid and interfacial transport in nano confinements. *Langmuir*, *31*(7), 2167–2179.

Kewen, L., & Roland, N. H. (2006). Generalized Scaling Approach for Spontaneous Imbibition: An Analytical Model. *SPE Reservoir Evaluation & Engineering*, *9*(3), 251–258.

Li, C., Xian, C., Shen, Y., Ge, H., & Liu, Y. (2022). Partial fractional differential model for gas-liquid spontaneous imbibition with special imbibition index: imbibition behavior and recovery analysis. *Journal of Petroleum Science and Engineering*, *209*.

Li, K., & Horne, R. N. (2004). An Analytical Scaling Method for Spontaneous Imbibition in Gas/Water/Rock Systems. *SPEJ*, *9*(3), 322–329.

Liu, H. H., Lai, B., & Chen, J. (2016). Unconventional spontaneous imbibition into shale matrix: Theory and a methodology to determine relevant parameters. *Transport in Porous Media*, *111*(1), 41–57.

Liu, H., Sun, S., Wu, R., Wei, B., & Hou, J. (2021). Pore-scale modeling of spontaneous imbibition in porous media using the lattice Boltzmann method. *Water Resources Research*, *57*(6), e2020WR029219.

Liu, Y., Cai, J., Sahimi, M., & Qin, C. (2020). A study of the role of microfractures in counter-current spontaneous imbibition by lattice Boltzmann simulation. *Transport in Porous Media*, *133*, 313–332.

Ma, S., Morrow, N. R., & Zhang, X. (1997). Generalized scaling of spontaneous imbibition data for strongly water-wet systems. *Journal of Petroleum Science and Engineering*, *18*, 165–178.

Mahdaviara, M., Sharifi, M., Bakhshian, S., & Shokri, N. (2022). Prediction of spontaneous imbibition in porous media using deep and ensemble learning techniques. *Fuel*, *329*(125349).

Mason, G., & Morrow, N. R. (2013). Developments in spontaneous imbibition and possibilities for future work. *Journal of Petroleum Science and Engineering*, *110*, 268–293.

Mattax, C. C., & Kyte. (1962). Imbibition Oil Recovery from Fractured, Water-Drive Reservoir. *Society of Petroleum Engineers Journal*, *2*(2), 177–184.

Mcwhorter, D. B., & Sunada, D. K. (1990). Exact Integral Solutions for Two-Phase Flow. *Water Resources Research*, *26*(3).

Meerschaert, M. M., & Sikorskii, A. (2019). Stochastic models for fractional calculus. *Walter de Gruyter GmbH & Co KG*, *43*.

Meng, Q., Zhao, L., Li, P., Yang, F., & Cai, J. (2022). Experiments and phase-field simulation of counter-current imbibition in porous media with different pore structure. *Journal of Hydrology*, *608*(127670).

Ning, X., Ewing, R., Hu, Q., Wang, Q., & Zhang, X. (2022). A new model for simulating the imbibition of a wetting-phase fluid in a matrix-fracture dual connectivity system. *Geofluids*, *2022*.

Pachepsky, Y., Timlin, D., & Rawls, W. (2003). Generalized Richards' equation to simulate water transport in unsaturated soils. *Journal of Hydrology*, *272*, 3–13.

Pan, B., Clarkson, C. R., Atwa, M., Tong, X., Debuhr, C., Ghanizadeh, A., & Birss, V. I. (2021). Spontaneous imbibition dynamics of liquids in partially-wet nano-porous media: experiment and theory. *Transport in Porous Media*, *137*(3), 555–574.

Pan, B., Clarkson, C. R., Younis, A., Song, C., Debuhr, C., Ghanizadeh, A., & Birss, V. I. (2022). New methods to evaluate impacts of osmotic pressure and surfactant on fracturing fluid loss and effect of contact angle on spontaneous imbibition data scaling in unconventional reservoirs. *Fuel*, *328*(125328).

Perfect, E., Brabazon, J. W., & Gates, C. H. (2020). Forward prediction of early-time spontaneous imbibition of water in unsaturated rock fractures. *Vadose Zone Journal*, *19*(1), e20056.

Qin, C. Z., Wang, X., Hefny, M., Zhao, J., Chen, S., & Guo, B. (2022). Wetting Dynamics of Spontaneous Imbibition in Porous Media: From Pore Scale to Darcy Scale. *Geophysical Research Letters*, *49*(4).

Rapoport, L. A. (1955). Scaling laws for use in design and operation of water-oil flow models. *Transactions of the AIME*, *204*(1), 143–150.

Richards, L. A. (1931). Capillary conduction of liquids through porous mediums. *Journal of Applied Physics*, *1*(5), 318–333.

Ruprecht, C., Pini, R., Falta, R., Benson, S., & Murdoch, L. (2014). Hysteretic trapping and relative permeability of CO2 in sandstone at reservoir conditions. *International Journal of Greenhouse Gas Control*, *27*, 15–27.

Schmid, K. (2012). Mathematical Analysis, Scaling and Simulation of Flow and Transport during immiscible Two-Phase Flow. *Diss. Heriot-Watt University*.

Schmid, K. S., & Geiger, S. (2012). Universal scaling of spontaneous imbibition for water-wet systems. *Water Resources Research*, *48*(3).

Shi, Y., Yassin, M. R., & Dehghanpour, H. (2018). A modified model for spontaneous imbibition of wetting phase into fractal porous media. *Colloids and Surfaces A: Physicochemical and Engineering Aspects*, *543*, 64–75.

Standnes, D. C. (2004). Experimental study of the impact of boundary conditions on oil recovery by co-current and counter-current spontaneous imbibition. *Energy and Fuels*, *18*(1), 271–282.

Sun, H. G., Meerschaert, M. M., Zhang, Y., Zhu, J., & Chen, W. (2013). A fractal Richards' equation to capture the non-Boltzmann scaling of water transport in unsaturated media. *Advances in Water Resources*, *52*, 292–295.

Sun, M., Yu, B., Hu, Q., Yang, R., Zhang, Y., & Li, B. (2017). Pore connectivity and tracer migration of typical shales in south China. *Fuel*, *203*, 32–46.

Van Genuchten, M. T. (1980). A closed-form equation for predicting the hydraulic conductivity of unsaturated soils. *Soil Science Society of America Journal* , *44*(5), 892–898.

Zahasky, C., & Benson, S. M. (2019). Spatial and Temporal Quantification of Spontaneous Imbibition. *Geophysical Research Letters*, *46*(21), 11972–11982.

Zhang, X., of Wyoming, U., & Morrow, N. R. (1996). Experimental Verification of a Modified Scaling Group for Spontaneous Imbibition. *SPE Reservoir Engineering*, *11*(4), 280–285.

Zhao, J., Qin, F., Fischer, R., Kang, Q., Derome, D., & Carmeliet, J. (2021). Spontaneous imbibition in a square tube with corner films: theoretical model and numerical simulation. *Water Resources Research*, *57(2)*(e2020WR029190).

Zhao, Y., Wu, Y., Dong, C., Han, S., Elsworth, D., & He, L. (2022). Hydraulic characterization and modeling of water diffusivity through direct neutron radiography measurement on unsaturated cracked sandstone. *International Journal of Heat and Mass Transfer*, *123256*.

Zhou, D., Jia, L., Kamath, J., & Kovscek, A. R. (2002). Scaling of counter-current imbibition processes in low-permeability porous media. *Journal of Petroleum Science and Engineering* , *3*, 61–74.